Properties of Dopants in HfO_x for Improving the Performance of Nonvolatile Memory

Dan Duncan,* Blanka Magyari-Köpe, and Yoshio Nishi

Department of Electrical Engineering, Stanford University, Stanford, California 94305, USA

(Received 26 April 2016; revised manuscript received 24 January 2017; published 24 March 2017)

Doping is an increasingly popular technique for improving the characteristics of cutting-edge HfO_x nonvolatile memory devices, but relatively few dopant species have been investigated. In this work, the properties of 50 different cation and anion dopants in HfO_x are explored using density-functional theory and are corroborated with experimental data. Depending on the atomic species, dopants are found to preferentially form on either substitutional or interstitial lattice sites and to reduce the formation energy of oxygen vacancies in the surrounding oxide. The behavior of cation dopants in HfO_x is also found to be well predicted by six properties: dopant valence, atomic radius, native-oxide enthalpy of formation, coordination number, magnetization, and charge transfer with the HfO_x lattice. These results can be used to optimize dopant selection for tuning of the switching characteristics of HfO_x-based resistance-change random-access-memory and conductive-bridge random-access-memory devices.

DOI: 10.1103/PhysRevApplied.7.034020

I. INTRODUCTION

Transition-metal-oxide resistance-change random-access memory (RRAM)—and hafnium oxide (HfO_2) in particular—shows great potential for applications in the next generation of nonvolatile memory [1] and neuromorphic computing [2]. RRAM devices are believed to switch states by forming and dissolving conductive filaments of oxygen vacancies (V_O's) [1]. They display many desirable properties, including low power, simple structure, fast switching speed (<10 ns), extreme scalability (<10 nm), and CMOS compatibility including 3D integration [3–5]. One of the most significant research areas for RRAM is reducing variability: batch to batch, device to device, and cycle to cycle [6,7]. Lack of control of the low-resistance state (LRS), high-resistance state (HRS), and intermediate-resistance states is a significant hurdle to achieving reproducible devices with high-bit density and multilevel switching [8]. Numerous techniques have been explored for improving RRAM device characteristics and variability, including bilayer stacks [9], pulse-shape optimization [10], nonlinear devices [11], and complementary device configurations [12].

One option for tuning device characteristics is doping. Doped RRAM devices have been shown to exhibit changes to forming voltage, SET voltage, power dissipation, on:off ratio, variability, retention, and endurance [7,8,13–20]. These changes occur because RRAM devices operate by the formation and annihilation of oxygen vacancy filaments, and doping can locally alter the energetics of V_O formation. Indeed, dopants that reduce V_O formation energy in their immediate vicinity have been found to encourage resistive switching [7,13,14,20].

The preferred lattice site of dopant ions is also expected to impact device behavior. This is the case because interstitial cation dopants are known to form conductive filaments of their own [21–23], and this phenomenon is used to make the cation-based analog of RRAM called conductive-bridge random-access memory (CBRAM). For RRAM devices, it is therefore desirable to have dopants that favor substitutional lattice sites, as these are unlikely to form cation filaments that compete with V_O-based ones.

We performed density-functional calculations for a total of 50 different candidate dopants: 42 cation, 5 anion, and 3 amphoteric. Dopant preference for substitutional and interstitial lattice sites and their effects on V_O formation energy are examined. While the focus here is on RRAM, both substitutional and interstitial dopants are identified in this work, with potential applications for both RRAM and CBRAM.

II. METHODS

Spin-polarized density-functional theory (DFT) calculations using the Vienna *ab initio* simulation package are carried out on monoclinic HfO_2 (m-HfO_2, space group $P21/c$). Projector augmented-wave pseudopotentials, periodic boundary conditions, and an energy cutoff of 367.38 eV are employed. k-point integration uses $2 \times 2 \times 2$ Γ-centered Monkhorst-Pack grids, and all ions are relaxed to an energy convergence of 10^{-3} eV/atom and forces less than 0.01 eV/Å per ion.

To maximize accuracy and performance, we use the LDA + U method described in Ref. [24], which has been used previously for calculations on rutile TiO_2 [25], substoichiometric HfO_2 [26,27], and doped HfO_2 [13]. The on-site Coulomb corrections used are $U^d = 6.6$ eV on the Hf $5d$ orbital and $U^p = 9.5$ eV on the O $2p$ orbital.

*duncand@alumni.stanford.edu

This approach has achieved accuracy in HfO_2 on a par with hybrid functionals such as HSE06 [28–30], and at the same speed as local-density approximation (LDA) and generalized-gradient approximation calculations, which do not otherwise accurately capture the electronic structure of HfO_2 [31–33].

A unit cell of m-HfO_2 contains 12 atoms: 4 sevenfold-coordinated Hf, 4 threefold-coordinated (3C) O, and 4 fourfold-coordinated (4C) O atoms. This work uses $3 \times 3 \times 3$ supercells measuring 15 Å to a side and containing 324 atoms. Cells are relaxed, containing either a single dopant ion or one dopant ion and one V_O, resulting in a dopant concentration of 2.8×10^{20} cm^{-3}.

Cation dopants are relaxed on Hf sites, anion dopants on O sites, and amphoteric dopants on both Hf and O sites. In addition, two unique interstitial sites are identified in the monoclinic cell. These sites are found by identifying trial sites where free space is maximized, then performing test relaxations of interstitials at all of the trial sites. Eight optimally favorable interstitial sites are identified, which can be further broken down into two sets of four identical sites. All dopants are relaxed at both of the unique interstitial sites.

III. DERIVATION OF EQUATIONS

The four defect types analyzed in this study are oxygen vacancies (V_O's), cation substitutional dopants (D_{Hf}), anion substitutional dopants (D_O), and interstitial dopants (D_I). For a cation substitutional dopant D_{Hf}, the formation reaction is usually written as

$$D_{Hf}\colon\ HfO_2 + D \Leftrightarrow (HfO_2)^{D_{Hf}} + Hf. \tag{1}$$

However, this formulation results in a defect formation energy that is a function of the chemical potential of hafnium, μ_{Hf}. Because deposition conditions are assumed to be O rich, and to facilitate comparison between different defect sites, the formation reaction of D_{Hf} can instead be written in terms of the chemical potential of oxygen, μ_O. The two equivalent formation reactions are depicted schematically in Fig. 1, and the final equations for defect formation are presented next.

Equations (2)–(5) give the formation reactions of the four defects of interest in HfO_2 with an O_2 ambient:

$$V_O\colon\ HfO_2 - \frac{1}{2}O_2 \Leftrightarrow (HfO_2)^{V_O} \tag{2}$$

$$D_{Hf}\colon\ \frac{n-1}{n}HfO_2 + D + O_2 \Leftrightarrow (HfO_2)^{D_{Hf}} \tag{3}$$

$$D_O\colon\ HfO_2 + D \Leftrightarrow (HfO_2)^{D_O} + \frac{1}{2}O_2 \tag{4}$$

$$D_I\colon\ HfO_2 + D \Leftrightarrow (HfO_2)^{D_I}, \tag{5}$$

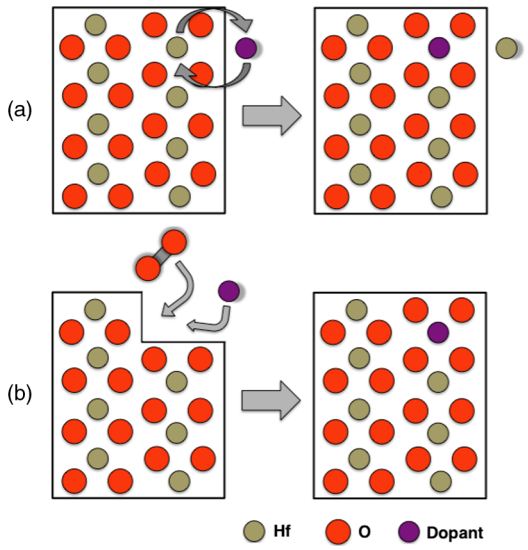

FIG. 1. (a) Formation of D_{Hf} by substitution with Hf depends on μ_{Hf}. (b) Formation of D_{Hf} by the addition of D and O_2 depends on μ_O instead.

where n is the number of formula units in the supercell (e.g., one unit cell of m-HfO_2 contains four formula units). For the formation of neutral defects described by Eqs. (2)–(5), we write the defect formation energy as follows:

$$V_O\colon\ E_{form}(V_O) = E(V_O) - \left[E_0 - \frac{1}{2}E(O_2)\right] \tag{6}$$

$$D_{Hf}\colon\ E_{form}(D_{Hf}) = E(D_{Hf}) - \left[\left(\frac{n-1}{n}\right)E_0 + E(D) + E(O_2)\right] \tag{7}$$

$$D_O\colon\ E_{form}(D_O) = E(D_O) - \left[E_0 + E(D) - \frac{1}{2}E(O_2)\right] \tag{8}$$

$$D_I\colon\ E_{form}(D_I) = E(D_I) - [E_0 + E(D)]. \tag{9}$$

Where $E_{form}(x)$ is the formation energy of defect x, $E(V_O)$ and $E(D_x)$ are the total energies of the defective HfO_2 supercells containing defects V_O and D_x, E_0 is the total energy of the pristine supercell, and $E(O_2)$ and $E(D)$ are the chemical potentials of O_2 and D.

Because the chemical potential of dopants varies widely by dopant species and experimental conditions, one final modification is made: the dependence of E_{form} on dopant chemical potential is eliminated. Therefore, we calculate E_r, the relative formation energy of each dopant at different sites. E_r depends on whether the dopant substitutes on the cation or anion site, but not on the dopant's chemical potential:

$$E_r(D_I, D_{\mathrm{Hf}}) = E_{\mathrm{form}}(D_I) - E_{\mathrm{form}}(D_{\mathrm{Hf}}) = E(D_I) - E(D_{\mathrm{Hf}}) + E(\mathrm{O}_2) - \frac{1}{n}E_0 \quad (10)$$

$$E_r(D_I, D_{\mathrm{O}}) = E_{\mathrm{form}}(D_I) - E_{\mathrm{form}}(D_{\mathrm{O}}) = E(D_I) - E(D_{\mathrm{O}}) - \frac{1}{2}E(\mathrm{O}_2). \quad (11)$$

$E_r(D_I, D_x) < 0$ eV indicates that the dopant D favors the interstitial site I over the substitutional site x, and $E_r(D_I, D_x) > 0$ eV indicates that the substitutional site is favored. In this form, E_r becomes a quantity entirely determined by variables that are easily obtained from DFT calculations.

For the case of amphoteric dopants, it is also useful to extend E_r to directly compare the Hf and O sites. The equation for this comparison is

$$E_r(D_{\mathrm{O}}, D_{\mathrm{Hf}}) = E_{\mathrm{form}}(D_{\mathrm{O}}) - E_{\mathrm{form}}(D_{\mathrm{Hf}}) = E(D_{\mathrm{O}}) - E(D_{\mathrm{Hf}}) + \frac{3}{2}E(\mathrm{O}_2) - \frac{1}{n}E_0. \quad (12)$$

Here, $E_r(D_{\mathrm{O}}, D_{\mathrm{Hf}}) < 0$ eV indicates that the O site is favored over the Hf site, and $E_r(D_{\mathrm{O}}, D_{\mathrm{Hf}}) > 0$ eV indicates that the Hf site is more favorable than the O site.

Finally, all three equations for E_r depend on the chemical potential of O. For results presented in the next section, a constant $\mu_{\mathrm{O}} = \frac{1}{2}E(\mathrm{O}_2) = -5.375$ eV is used, which corresponds to the formation reactions taking place in an O_2 ambient. A higher μ_{O}, such as formation in the presence of oxygen plasma, would cause two shifts in the relative formation energy: $E_r(D_I, D_{\mathrm{Hf}})$ would become more positive, making the cation site more favorable relative to the interstitial site; and $E_r(D_I, D_{\mathrm{O}})$ would become less positive, making the interstitial site more favorable relative to the anion site. By extension, this also means that a higher μ_{O} results in a higher $E_r(D_{\mathrm{O}}, D_{\mathrm{Hf}})$, meaning that the cation site becomes more favorable relative to the anion site.

IV. RESULTS AND DISCUSSION

The calculated relative formation energies for cation, anion, and amphoteric dopants are shown in Figs. 2, 3, and 4, respectively. E_r is found to depend strongly on the dopant ion's valence. The more isovalent an ion is with the species it is replacing, the more stable it is on the substitutional site. Conversely, more heterovalent ions are more stable on interstitial sites.

For anion dopants, the substitutional site is always favored. In addition, both interstitial sites are found to be energetically equivalent for all anion dopants. As a result, Fig. 3 plots E_r for only one interstitial site.

The amphoteric dopants also include $E_r(D_{\mathrm{O}}, D_{\mathrm{Hf}})$. At a constant $\mu_{\mathrm{O}} = \frac{1}{2}E(\mathrm{O}_2) = -5.375$ eV, it is found that H_{O}, C_{O}, and Si_{Hf} are the most favored defects. In a more reactive environment with a higher μ_{O}, the Hf site would become relatively more favorable. For hydrogen, $\mu_{\mathrm{O}} > -2.75$ eV makes H_I more favorable than H_{O}. For carbon, $\mu_{\mathrm{O}} > -3$ eV results in C_I becoming dominant. For silicon, Si_{Hf} is favored for all values of μ_{O}. There is also no value of μ_{O} that results in H_{Hf} or C_{Hf} being favored.

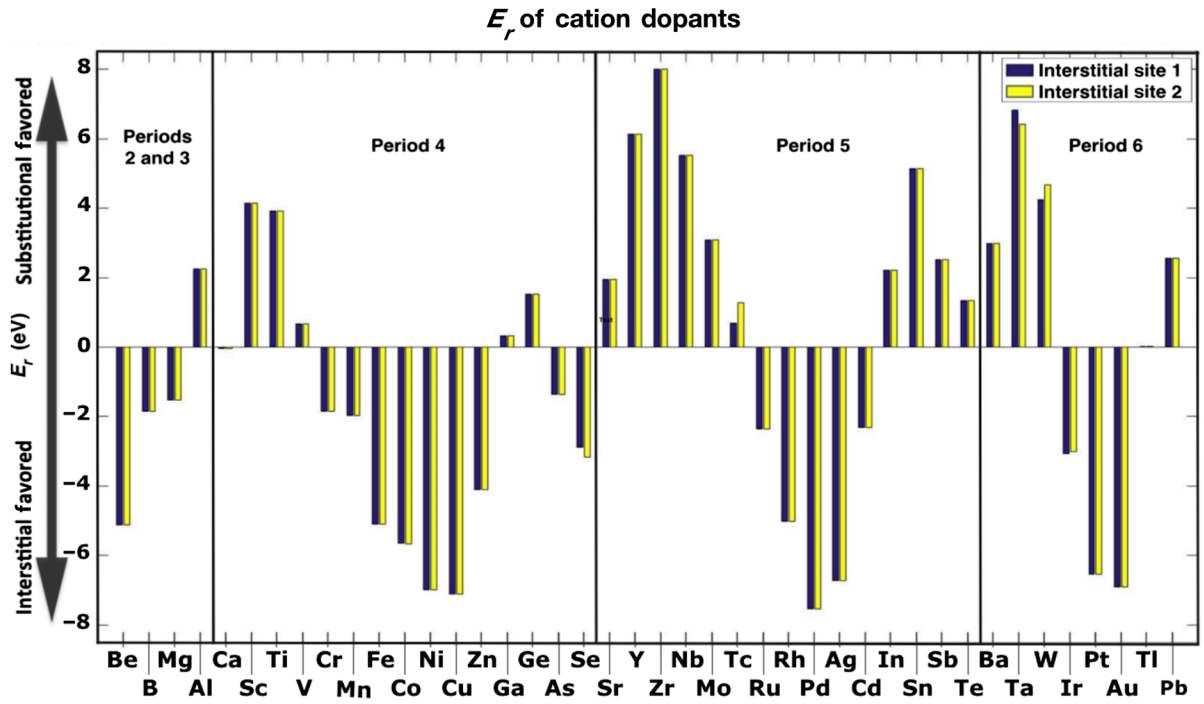

FIG. 2. $E_r(D_I, D_{\mathrm{Hf}})$ for cation dopants at two different interstitial sites in m-HfO_2.

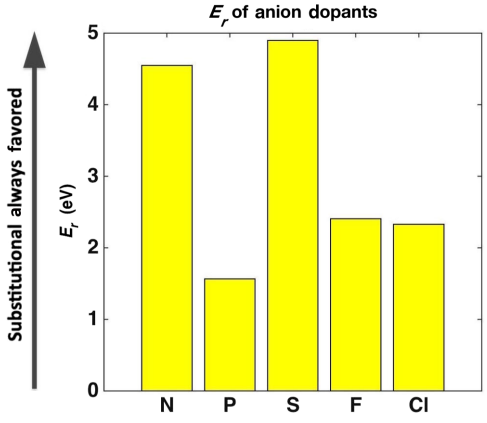

FIG. 3. $E_r(D_I, D_O)$ for anion dopants in m-HfO_2.

These calculations agree well with existing experimental and theoretical data. For example, Al [7,34], Si [18], and Zr [13,14] are seen to favor cation substitutional sites in HfO_2. Interstitial sites are favored by Ag [21], B [35], Cu [13,23], and Ni [22]. H [19,36], F [37], and N [20,38] are known to favor anion substitutional sites, all in agreement with the results presented here. For many of the other dopants investigated in this study, no experimental data have been reported, and these results would be useful in guiding future experiments. In general, it is expected that strongly substitutional dopants are suitable for RRAM applications, while strongly interstitial ones would be suitable for CBRAM.

Figure 2 also shows a clear periodicity in E_r of cation dopants, pointing to isovalency with Hf as being a driving factor. This trend is examined further using the density of states (DOS). In Fig. 5, the site-projected DOS of undoped m-HfO_2 is plotted, and it can be seen that the valence band of m-HfO_2 is mainly made up of O $2p$ states, while the conduction band is mainly Hf $5d$ states. Then, in Fig. 6, the site-projected DOS of doped m-HfO_2 is plotted for dopants from period 5. To clearly show the contributions of the

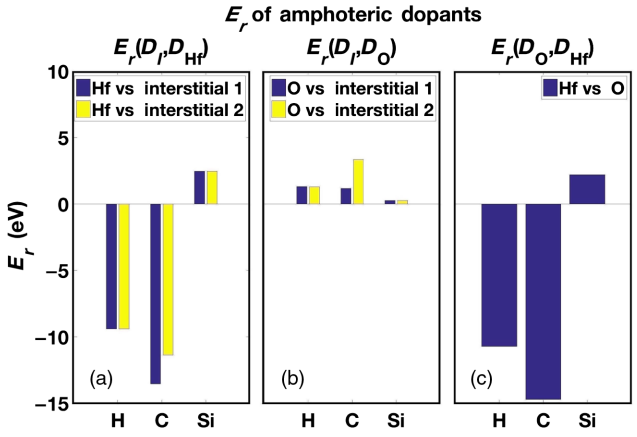

FIG. 4. (a) $E_r(D_I, D_{Hf})$, (b) $E_r(D_I, D_O)$, and (c) $E_r(D_O, D_{Hf})$ for amphoteric dopants in m-HfO_2.

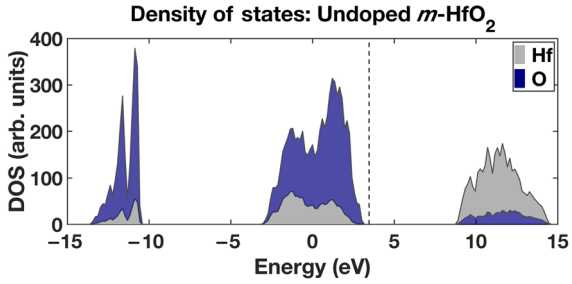

FIG. 5. Site-projected density of states of undoped m-HfO_2.

dopants, these plots are enlarged to just the range of energies between the valence band and the conduction band. The plots show the most substitutionally stable dopants, such as Zr and Sn, cause minimal perturbation to the DOS when in the substitutional site. In addition, the perturbations of substitutionally stable dopants are concentrated in the conduction band. Since the HfO_2 conduction band consists mainly of Hf states, this means that the dopants interact with the surrounding lattice similarly to the Hf ions they replaced, minimizing disruption to the crystal.

By contrast, dopants that are the most stable interstitially tend to exhibit smaller overall perturbations to the DOS when on the interstitial site, such as the case of Ag. They also tend to introduce many midgap or valence-band states when located on the substitutional Hf site, such as that seen for Pd. Because Hf mainly contributes to the conduction band, contributions to the valence band in the substitutional site are unfavorable. Finally, comparing the interstitial configuration to the substitutional, the DOS perturbations are more pronounced at the band edges than at midgap for the interstitial case. Because this is an interstitial site, there is a preference for shallow electronic states over deep ones, but no preference for a particular band edge. In Figs. 7 and 8, the qualitative concept of DOS perturbations are formally quantified as charge perturbation.

Next, because cation dopants exhibit such a strong dependence of E_r on dopant species, the trends underlying cation E_r are investigated. Six quantities are identified as drivers of E_r: (i) isovalency with Hf, (ii) dopant atomic radius relative to Hf, (iii) dopant native-oxide enthalpy of formation, (iv) the change in coordination number going from the dopant's native oxide to HfO_2, (v) the magnetization of the doped system, and (vi) the charge perturbation caused by the dopant at the Hf site.

Quantities (i)–(iii) are readily available in the literature. For quantities (i) and (ii), it is expected that dopants which are chemically and physically similar to Hf will be more likely to favor the Hf lattice site. For quantity (iii), dopants that strongly favor forming their own oxides are also likely to favor the substitutional site in HfO_2, where they can be fully coordinated with surrounding O ions.

Quantity (iv), the change in coordination number of dopant D, is used because dopants may favor sites with coordination most similar to their native oxides. Change in

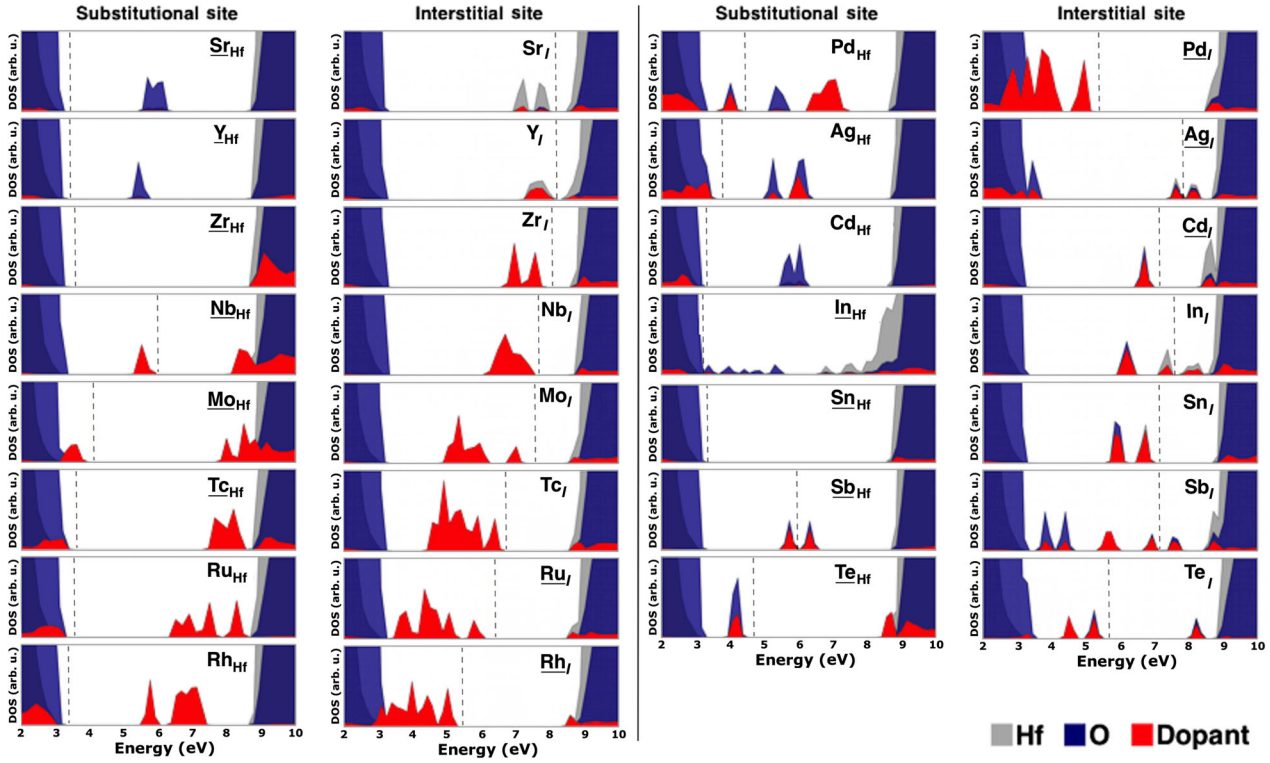

FIG. 6. The site-projected density of states of doped m-HfO_2 for period-5 dopants at substitutional and interstitial sites. The most stable lattice site, D_{Hf} or D_I, is underlined for each species.

coordination is calculated from three quantities: the coordination of D in its native oxide (D_0), the coordination of D in the substitutional site in HfO_2 (D_{Hf}), and the coordination of D in the interstitial site in HfO_2 (D_I):

$$\Delta\mathrm{CN} = |D_I - D_0| - |D_{\mathrm{Hf}} - D_0|. \tag{13}$$

For quantity (v), it is found that dopants favored sites of lower magnetization, possibly due to state splitting in the DOS, whereby the magnetic moment pushed some electron states to higher energies and increased the total energy of magnetic systems.

Quantity (vi), the charge perturbation, formally quantifies the DOS perturbation discussed in Fig. 5. The site-projected DOS is integrated up to the Fermi level for every ion in the lattice, and the ion's nuclear charge subtracted, to obtain the net charge of all ions in the system. Thus, the total charge Q_i on ion i is given by

$$Q_i = Z_i - \int_{-\infty}^{E_F} N_i(E)dE, \tag{14}$$

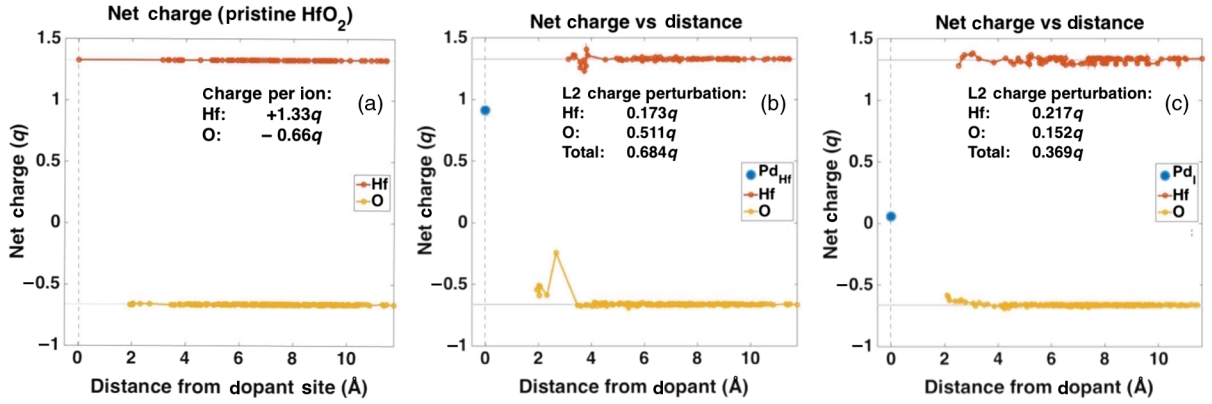

FIG. 7. Charge perturbation in the (a) undoped, (b) Pd_{Hf}, and (c) Pd_I systems. Pd introduces less perturbation in the interstitial site, which is its favored location.

where Z_i is the nuclear charge and $N_i(E)$ is the site-projected DOS on ion i. This calculation is done for the undoped and doped systems, and the total change in charge of the ions in the doped system is calculated. Plots for Pd are shown in Fig. 7, and they match well with the DOS plot for Pd in Fig. 6.

With all six quantities formally defined, E_r for the cation dopants is approximated as a linear function of each quantity, with plots shown in Fig. 8. The correlation coefficient R between each quantity and E_r is seen to vary from $0.3526 < |R| < 0.7894$. So, while correlations are present, no single quantity alone could be used to determine E_r.

In order to obtain a better prediction, E_r is approximated as a weighted sum of each of the six quantities above. For a given dopant D, $E_r(D)$ is estimated to be

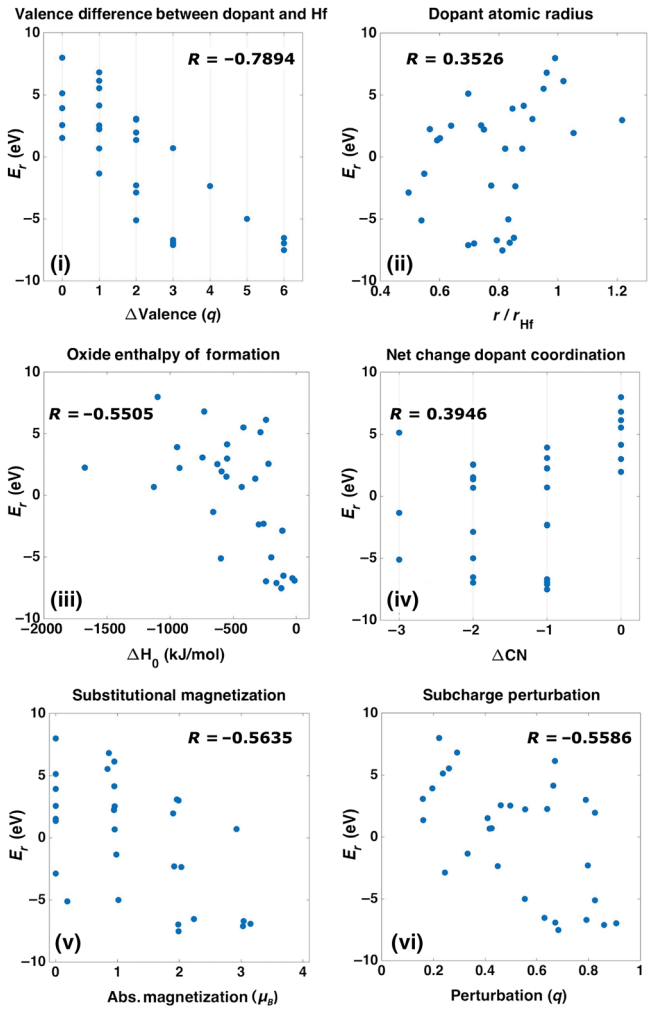

FIG. 8. The correlation between the cation dopant E_r and (i) the isovalency with Hf, (ii) the atomic radius relative to Hf, (iii) the native-oxide enthalpy of formation, (iv) the change in coordination, (v) the absolute magnetization, and (vi) the total-charge perturbation.

$$\hat{E}_r(D) = (Q_D)^T W, \tag{15}$$

where $\hat{E}_r(D)$ is the estimated relative formation energy of dopant D, $Q_D \in \mathbb{R}^{6\times 1}$ is the vector of the six quantities for dopant D, and $W \in \mathbb{R}^{6\times 1}$ is the vector of weights, where the same weights are applied to all dopants. The weight vector is found by combining the data for all N cation dopants under consideration into a vector $E_r \in \mathbb{R}^{N\times 1}$ and matrix $Q \in \mathbb{R}^{6\times N}$. The least-squares best fit for W can then be solved for analytically:

$$W = (QQ^T)^{-1}QE_r = (Q^T)^+ E_r, \tag{16}$$

where $X^+ \equiv (X^T X)^{-1}X^T$ is the Moore-Penrose pseudoinverse of X.

Therefore, the composite function of six weights and six parameters can be written as

$$\hat{E}_r(D) = W_V|\Delta V_D| + W_r\frac{r_D}{r_{\mathrm{Hf}}} + W_{\mathrm{H}}\Delta \mathrm{H}_0(D\mathrm{O}_X) + W_{\mathrm{CN}}\Delta\mathrm{CN} + W_M|M_D| + W_Q\sqrt{\sum(\Delta Q)^2}, \tag{17}$$

where ΔV_D is the difference in valence between D and Hf, r_D and r_{Hf} are the atomic radii of D and Hf, $\Delta \mathrm{H}_0(D\mathrm{O}_X)$ is the enthalpy of formation of D's native oxide, ΔCN is the change in coordination number as defined in Eq. (13), M_D is the absolute magnetization of the substitutionally doped system, and $\sqrt{\sum(\Delta Q)^2}$ is the ℓ^2 norm of the charge perturbation over all of the ions in the substitutionally doped cell. Finally, the six W terms are the weights for these six quantities.

The calculated optimal weights W are given in Table I. When all six quantities are combined into a single composite function, they are able to estimate E_r with $R = 0.9528$, as shown in Fig. 9. In addition, because W_V, W_r, and W_{H} depend solely upon experimental values available in the literature and do not require expensive DFT calculations, a second reduced composite function is calculated with just these three weights. It is found to still estimate E_r with $R = 0.8709$ and is plotted in Fig. 10. In

TABLE I. The calculated weights W for the full and reduced composite functions predicting $E_r(D)$.

Weight	Units	Full composite function	Reduced composite function
W_V	eV/q	−1.1374	−2.0953
W_r	eV	8.4436	4.7805
W_{H}	eV/(kJ/mol)	-2.044×10^{-3}	-1.541×10^{-3}
W_{CN}	eV	1.0439	0
W_M	eV/μ_B	−1.3683	0
W_Q	eV/q	−4.3894	0

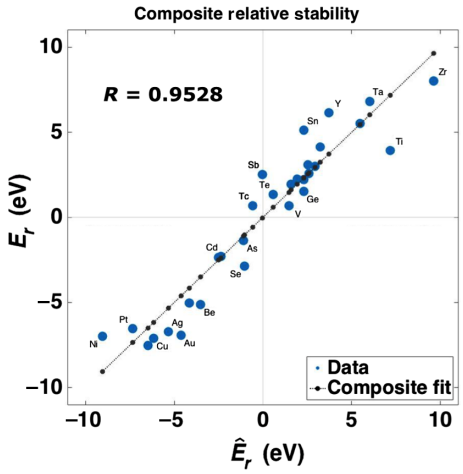

FIG. 9. Comparison of the actual $E_r(D)$ to the estimate $\hat{E}_r(D)$ found using the full composite function.

summary, these six quantities—particularly the three known *a priori*—can provide a reliable fitting of dopant behavior in HfO_2, and they may also be useful in predicting dopant behavior in other transition-metal oxides.

With the preferred lattice sites of all dopants calculated, the effect of dopants on V_O formation energy is investigated next. This investigation is done by placing a dopant ion at its most favorable substitutional site, then using Eq. (6) to calculate the formation energy of a neutral V_O at the nearest 3C and 4C oxygen sites. Because substitutional dopants are expected to be the most useful for RRAM devices, all of the strongly substitutional dopants, defined as those with $E_r > 1$ eV, are included in the calculation. To provide a broader sampling of dopant types, particularly the strongly *n*-type ones, several interstitially stable cation dopants are included as well. As seen in Figs. 11 and 12, the presence of dopants generally reduces the formation energy of nearby V_O's, but the magnitude of the reduction depends upon the dopant species.

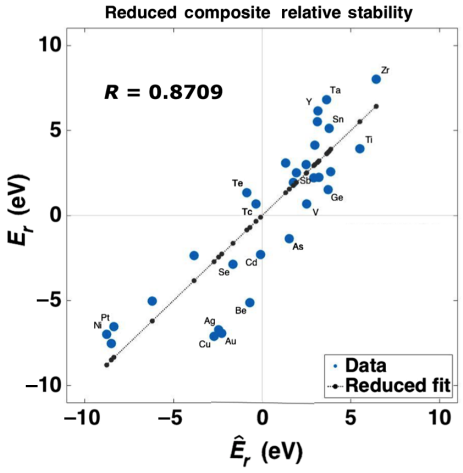

FIG. 10. Comparison of $E_r(D)$ to $\hat{E}_r(D)$ found using the reduced composite function.

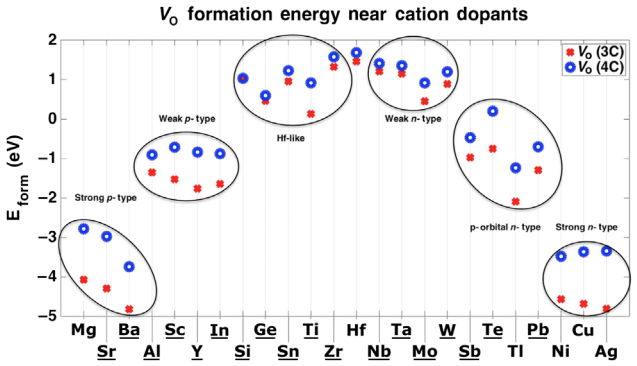

FIG. 11. Formation energy of neutral V_O's next to cation substitutional dopant defects (D_{Hf}). The names of strongly substitutional dopant species are underlined.

It is found that the effect of cation dopants on V_O formation energy depend heavily upon their valence relative to Hf, with strongly *n*-type and strongly *p*-type dopants causing the greatest reductions in V_O formation energy. The effect of anions on V_O formation is generally weaker and less affected by the particular dopant species than those of cations. For both cation and anion dopants, the reduction in the V_O E_{form} is found to extend into a region of about 4 Å around each dopant.

The reduction of the V_O E_{form} by dopants on interstitial sites is also calculated. It is found to be uniformly smaller than the reduction caused by dopants on substitutional sites, and also not to vary strongly with dopant species. This is consistent with the experimental result that interstitially doped devices are dominated by metal-cation filaments instead of V_O filaments [21–23].

At the RRAM device level, the forming voltage (V_{form}) and the on:off ratio are two properties that could be expected to be directly affected by changes in V_O formation energy. V_{form} is the voltage at which resistive switching is initialized in a new RRAM device. A dopant that lowers the V_O E_{form} will increase the initial concentration of V_O's in

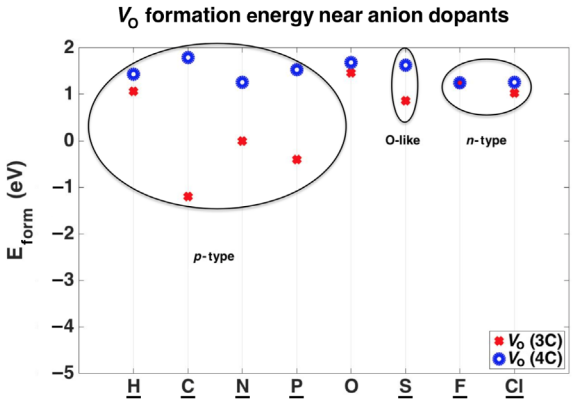

FIG. 12. Formation energy of neutral V_O's next to anion substitutional dopant defects (D_O).

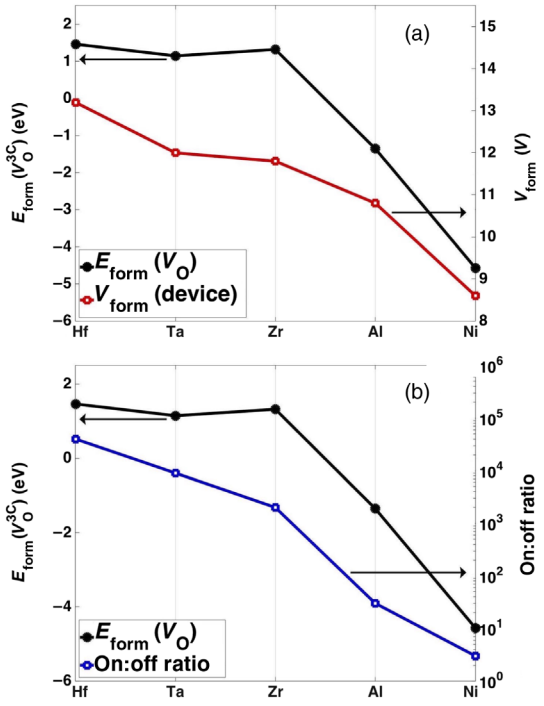

FIG. 13. Comparisons of calculation results (the black curves) with experimental data (the red and blue curves) [13] for (a) the RRAM device V_{form} and (b) the RRAM device on:off ratio both show a strong correlation between the V_O E_{form} and macroscopic RRAM device properties. Dopants are arranged in order of descending V_{form}.

the pristine device, making it easier to induce switching. Thus, a lower V_O E_{form} would be expected to reduce the V_{form}.

The on:off ratio is the ratio of the RRAM device resistance in the HRS to that of the LRS. A reduced V_O E_{form} is expected to increase current leakage in the HRS due to the presence of excess V_O percolation paths in the oxide bulk, reducing the HRS resistance. Thus, doping that lowers the V_O E_{form} would also be expected to lower the on:off ratio.

In Fig. 13, calculated dopant effects on the V_O E_{form} are compared to experimental data for both the V_{form} and the on:off ratio in doped RRAM devices [13]. As predicted, the V_{form} and the on:off ratio are both found to correlate strongly with the V_O E_{form}'s calculated here. Further corroboration is obtained by a comparison to other experimental work on cation dopants, such as that found in Refs. [7,17], which showed similar relationships between dopant species and RRAM device properties for the cases of Zr, Ge, Ta, Al, and Ni.

In addition to reducing the E_{form} of nearby V_O's, anion dopants may passivate existing V_O's. This possibility is confirmed experimentally for H [19,36], N [7,20,38], and F [37], predicted here to be anion dopants, which are all found to passivate existing V_O's in HfO_2.

From these calculations, it is predicted that Sr and Ba have the strongest effects of all substitutional dopants,

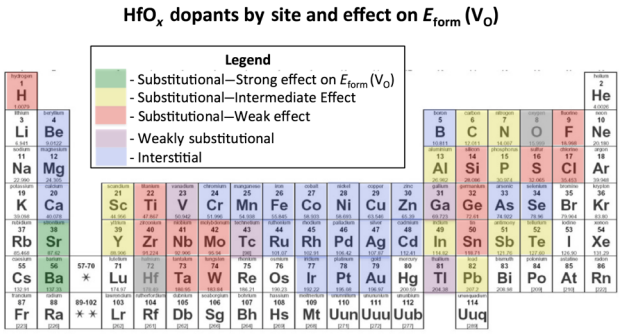

FIG. 14. Summary of dopants analyzed in this work. Weakly substitutional dopants are defined as those that favor the substitutional site over the interstitial one by less than 1 eV.

while others exhibit a range of smaller effects. In addition, many interstitial dopants are found which could be candidates for future HfO_2-based CBRAM devices, such as Pd. Our results are summarized in Fig. 14.

V. CONCLUSION

In this work, we derive equations for and calculate the preferred lattice sites of 50 different dopants in monoclinic HfO_2. Each dopant species is found to favor either the Hf, O, or interstitial site, and this relative formation energy is found to be reliably estimated by a combination of dopant valence, atomic radius, native-oxide enthalpy of formation, change in coordination, magnetization, and charge perturbation. Dopants favoring substitutional sites are predicted to be good candidates for RRAM devices, while those favoring interstitial ones could be candidates for CBRAM devices. It is also found that dopants modify the formation energy of nearby oxygen vacancies, with some demonstrating substantially stronger effects than others. Experimental data verify that the magnitude of this effect is directly correlated with changes in RRAM device properties.

This work demonstrates alternative guidelines for tuning the behavior of doped resistance-change memory devices, where dopants can be chosen based upon both their preferred lattice sites and how strongly they affect the surrounding lattice. Trends analyzed here are also general and could easily apply to doping in other oxides. Finally, we categorize dopants by lattice site and effect on V_O formation into a periodic table of dopants to guide future experiments on RRAM and CBRAM devices.

ACKNOWLEDGMENTS

This work was supported by the Stanford Nonvolatile Memory Technology Research Initiative (NMTRI), the Extreme Science and Engineering Discovery Environment (XSEDE) Allocation No. TG-DMR110086, and the Texas Advanced Computing Center (TACC).

[1] L. Goux, P. Czarnecki, Y. Y. Chen, L. Pantisano, X. P. Wang, R. Degraeve, B. Govoreanu, M. Jurczak, D. J. Wouters, and L. Altimime, Evidences of oxygen-mediated resistive-switching mechanism in TiN/HfO_2/Pt cells, Appl. Phys. Lett. **97**, 243509 (2010).

[2] S. Yu, Y. Wu, R. Jeyasingh, D. Kuzum, and H. S. P. Wong, An electronic synapse device based on metal oxide resistive switching memory for neuromorphic computation, IEEE Trans. Electron Devices **58**, 2729 (2011).

[3] R. Waser, R. Dittmann, G. Staikov, and K. Szot, Redox-based resistive switching memories—Nanoionic mechanisms, prospects, and challenges, Adv. Mater. **21**, 2632 (2009).

[4] H.-S. P. Wong, H. Y. Lee, S. Yu, Y. S. Chen, Y. Wu, P. S. Chen, B. Lee, F. T. Chen, and M. J. Tsai, Metal oxide RRAM, Proc. IEEE **100**, 1951 (2012).

[5] F. T. Chen, Y. S. Chen, T. Y. Wu, and T. K. Ku, Write scheme allowing reduced LRS nonlinearity requirement in a 3D-RRAM array with selector-less 1TNR architecture, IEEE Electron Device Lett. **35**, 223 (2014).

[6] S. Yu and H.-S. P. Wong, Characterization and modeling of the conduction and switching mechanisms of HFO_x based RRAM, MRS Online Proc. Libr. **1631**, mrsf13-1631-p04-03 (2014).

[7] D. Ning, P. Hua, and W. Wei, Effects of different dopants on switching behavior of HfO_2-based resistive random access memory, Chin. Phys. B **23**, 107306 (2014).

[8] Y. S. Chen, B. Chen, B. Gao, L. F. Liu, X. Y. Liu, and J. F. Kang, Well controlled multiple resistive switching states in the Al local-doped HfO_2 resistive random access memory device, J. Appl. Phys. **113**, 164507 (2013).

[9] K. Seo, I. Kim, S. Jung, M. Jo, S. Park, J. Park, J. Shin, K. P. Biju, J. Kong, K. Lee, B. Lee, and H. Hwang, Analog memory and spike-timing-dependent plasticity characteristics of a nanoscale titanium oxide bilayer resistive switching device, Nanotechnology **22**, 254023 (2011).

[10] J. Song, D. Lee, J. Woo, Y. Koo, E. Cha, S. Lee, J. Park, K. Moon, S. H. Misha, A. Prakash, and H. Hwang, Effects of reset current overshoot and resistance state on reliability of RRAM, IEEE Electron Device Lett. **35**, 636 (2014).

[11] L. Zhang, A. Redolfi, C. Adelmann, S. Clima, I. P. Radu, Y. Y. Chen, D. J. Wouters, G. Groeseneken, M. Jurczak, and B. Govoreanu, Ultrathin metal/amorphous-silicon/metal diode for bipolar RRAM selector applications, IEEE Electron Device Lett. **35**, 199 (2014).

[12] O. Kavehei, E. Linn, L. Nielen, S. Tappertzhofen, E. Skafidas, I. Valov, and R. Waser, An associative capacitive network based on nanoscale complementary resistive switches for memory-intensive computing, Nanoscale **5**, 5119 (2013).

[13] L. Zhao, S. W. Ryu, A. Hazeghi, D. Duncan, B. Magyari-Köpe, and Y. Nishi, in *Proceedings of the Symposium on VLSI Technology, Kyoto, Japan, 2013* (IEEE, New York, 2013), p. T106.

[14] Z. Yuanyang, W. Jiayu, X. Jianbin, Y. Fei, L. Qi, and D. Yuehua, Metal dopants in HfO_2-based RRAM: First principle study, J. Semicond. **35**, 042002 (2014).

[15] B. Gao, H. W. Zhang, S. Yu, B. Sun, L. F. Liu, X. Y. Liu, Y. Wang, R. Q. Han, J. F. Kang, B. Yu, and Y. Y. Wang, in *Proceedings of the Symposium on VLSI Technology, Kyoto, Japan, 2009* (IEEE, New York, 2009), p. 30.

[16] C.-S. Peng, W.-Y. Chang, Y.-H. Lee, M.-H. Lin, F. Chen, and M.-J. Tsai, Improvement of resistive switching stability of HfO_2 films with Al doping by atomic layer deposition, Electrochem. Solid-State Lett. **15**, H88 (2012).

[17] Z. Wang, W. G. Zhu, A. Y. Du, L. Wu, Z. Fang, X. A. Tran, W. J. Liu, K. L. Zhang, and H. Y. Yu, Highly uniform, self-compliance, and forming-free ALD HfO_2-based RRAM with Ge doping, IEEE Trans. Electron Devices **59**, 1203 (2012).

[18] D. Panda, C.-Y. Huang, and T.-Y. Tseng, Resistive switching characteristics of nickel silicide layer embedded HfO_2 film, Appl. Phys. Lett. **100**, 112901 (2012).

[19] S. Kim, D. Lee, J. Park, S. Jung, W. Lee, J. Shin, J. Woo, G. Choi, and H. Hwang, Defect engineering: Reduction effect of hydrogen atom impurities in HfO_2-based resistive-switching memory devices, Nanotechnology **23**, 325702 (2012).

[20] H. Xie, Q. Liu, Y. Li, H. Lv, M. Wang, X. Liu, H. Sun, X. Yang, S. Long, S. Liu, and M. Liu, Nitrogen-induced improvement of resistive switching uniformity in a HfO_2-based RRAM device, Semicond. Sci. Technol. **27**, 125008 (2012).

[21] G. Palma, E. Vianello, O. Thomas, H. Oucheikh, S. Onkaraiah, A. Toffoli, C. Carabasse, G. Molas, and B. De Salvo, in *Proceedings of the 43rd European Solid-State Device Research Conference (ESSDERC), Bucharest, 2013*, edited by C. Bulucea (IEEE, New York, 2013), p. 264.

[22] K. L. Pey, N. Raghavan, X. Wu, M. Bosman, X. X. Zhang, and K. Li, in *IEEE International Conference on Electron Devices and Solid-State Circuits (EDSSC), Chengdu, China, 2014* (IEEE, New York, 2014), p. 1.

[23] T. L. Tsai, H. Y. Chang, F. S. Jiang, and T. Y. Tseng, Impact of post-oxide deposition annealing on resistive switching in HfO_2-based RRAM and conductive-bridge RAM devices, IEEE Electron Device Lett. **36**, 1146 (2015).

[24] D. Duncan, B. Magyari-Köpe, and Y. Nishi, Hydrogen doping in HfO_2 resistance change random access memory, Appl. Phys. Lett. **108**, 043501 (2016).

[25] S.-G. Park, B. Magyari-Köpe, and Y. Nishi, Electronic correlation effects in reduced rutile TiO_2 within the LDA + U method, Phys. Rev. B **82**, 115109 (2010).

[26] D. Duncan, B. Magyari-Köpe, and Y. Nishi, Filament-induced anisotropic oxygen vacancy diffusion and charge trapping effects in hafnium oxide RRAM, IEEE Electron Device Lett. **37**, 400 (2016).

[27] D. Duncan, B. Magyari-Kope, and Y. Nishi, *Ab initio* modeling of the resistance switching mechanism in RRAM devices: Case study of hafnium oxide (HfO_2), MRS Online Proc. Libr. **1430**, mrss12-1430-e11-01 (2012).

[28] T.-T. Jiang, Q.-Q. Sun, Y. Li, J.-J. Guo, P. Zhou, S.-J. Ding, and D. W. Zhang, Towards the accurate electronic structure descriptions of typical high-constant dielectrics, J. Phys. D **44**, 185402 (2011).

[29] M. Jain, J.R Chelikowsky, and S.G Louie, Quasiparticle Excitations and Charge Transition Levels of Oxygen Vacancies in Hafnia, Phys. Rev. Lett. **107**, 216803 (2011).

[30] S. J. Clark, L. Lin, and J. Robertson, On the identification of the oxygen vacancy in HfO_2, Microelectron. Eng. **88**, 1464 (2011).

[31] T. V. Perevalov, V. A. Gritsenko, S. B. Erenburg, A. M. Badalyan, H. Wong, and C. W. Kim, Atomic and electronic structure of amorphous and crystalline hafnium oxide: X-ray photoelectron spectroscopy and density functional calculations, J. Appl. Phys. **101**, 053704 (2007).

[32] X. Zhao and D. Vanderbilt, First-principles study of structural, vibrational, and lattice dielectric properties of hafnium oxide, Phys. Rev. B **65**, 233106 (2002).

[33] K.-H. Xue, P. Blaise, L. R. C. Fonseca, G. Molas, E. Vianello, B. Traore, B. De Salvo, G. Ghibaudo, and Y. Nishi, Grain boundary composition and conduction in HfO_2, Appl. Phys. Lett. **102**, 201908 (2013).

[34] Z. F. Hou, X. G. Gong, and Q. Li, Energetics and electronic structure of aluminum point defects in HfO_2: A first-principles study, J. Appl. Phys. **106**, 014104 (2009).

[35] C.-L. Liu, *Ab initio* modeling of boron and oxygen diffusion in polycrystalline HfO_2 films, Phys. Status Solidi B **233**, 18 (2002).

[36] E. Efthymiou, S. Bernardini, J. F. Zhang, S. N. Volkos, B. Hamilton, and A. R. Peaker, Reliability degradation of thin HfO_2/SiO_2 gate stacks by remote RF hydrogen and deuterium plasma treatment, Thin Solid Films **517**, 207 (2008).

[37] W. Chen, Q.-Q. Sun, S.-J. Ding, D. W. Zhang, and L.-K. Wang, First principles calculations of oxygen vacancy passivation by fluorine in hafnium oxide, Appl. Phys. Lett. **89**, 152904 (2006).

[38] G. Shang, P. W. Peacock, and J. Robertson, Stability and band offsets of nitrogenated high-dielectric-constant gate oxides, Appl. Phys. Lett. **84**, 106 (2004).